Dynamic Substrate for the Physical Encoding of Sensory Information in Bat Biosonar

Rolf Müller,[1,*] Anupam K. Gupta,[1] Hongxiao Zhu,[2] Mittu Pannala,[1] Uzair S. Gillani,[3] Yanqing Fu,[4] Philip Caspers,[1] and John R. Buck[5]

[1]*Department of Mechanical Engineering, Virginia Tech, Blacksburg, Virginia 24061, USA*
[2]*Department of Statistics, Virginia Tech, Blacksburg, Virginia 24061, USA*
[3]*Department of Electrical and Computer Engineering, Virginia Tech, Blacksburg, Virginia 24061, USA*
[4]*Department of Biomedical Engineering and Mechanics, Virginia Tech, Blacksburg, Virginia 24061, USA*
[5]*Electrical and Computer Engineering Department, University of Massachusetts Dartmouth, Dartmouth, Massachusetts 02747, USA*

(Received 29 April 2016; published 11 April 2017)

Horseshoe bats have dynamic biosonar systems with interfaces for ultrasonic emission (reception) that change shape while diffracting the outgoing (incoming) sound waves. An information-theoretic analysis based on numerical and physical prototypes shows that these shape changes add sensory information (mutual information between distant shape conformations <20%), increase the number of resolvable directions of sound incidence, and improve the accuracy of direction finding. These results demonstrate that horseshoe bats have a highly effective substrate for dynamic encoding of sensory information.

DOI: 10.1103/PhysRevLett.118.158102

Like many hearing systems in biology, bat biosonar [1] encodes information about the presence [2], location [3], and characteristics of sound sources [4,5] in the environment. However, unlike many of its peers, bat biosonar by itself has the proven capability of encoding sensory information sufficient for rapid navigation in three dimensions, often in highly complicated environments [6]. The sites of ultrasound emission and reception are critical stages for the encoding of this information, because they are the only places where direction-dependent acoustic diffraction can occur [7]. Hence, structures positioned at these sites provide the sole physical substrate for the encoding of sensory information related to target direction. Probably because of this pivotal functional position, many bat species have evolved elaborate baffle shapes that diffract their ultrasonic pulses upon emission (noseleaves, in species with nasal emission) as well as during reception (pinnae). In horseshoe bats (family *Rhinolophidae*, [8]), for instance, shape features of the noseleaves [9] and the pinnae [10] have been linked to the distribution of the emitted energy and the receiver sensitivity as a function of direction (beam patterns). In recent years, a growing body of evidence has accumulated to suggest that, beyond their static geometric complexity, the noseleaves and pinnae of horseshoe bats have a prominent dynamic dimension [11]. Fast dynamic shape changes that go beyond rotations of static shapes [12,13] have been demonstrated to occur in both interface structures, noseleaves [14,15] and pinnae [16,17]. Along with the dynamic changes to the interface shapes, changes to the emission beam patterns during natural biosonar behaviors have been reported, but the underlying acoustic mechanisms remain unclear [18]. Evidence from several sources supports the hypothesis that the shape changes in the biosonar interfaces play a functional role: (i) the shape changes are effected by elaborate muscular actuation mechanisms [16,19], (ii) bats control the dynamic shape configuration sequences based on behavioral context [14,16], (iii) shape deformations coincide with ultrasonic diffraction in time [14,15], (iv) the magnitudes of the shape changes are significant compared to the transmitted wavelength [14,15,17]. In accordance with (iv), noseleaf and pinna deformations in horseshoe bats have been predicted to produce qualitative beam pattern changes [15,17,20]. Similar changes have been demonstrated experimentally with biomimetic reproductions of noseleaves [21] and pinnae [10,22]. In these experiments, the shape deformations resulted in time-variant device characteristics [21,23]. In the frequency domain, the beam patterns typically alternated between a concentration of sensitivity in a single main lobe and scattering among local maxima (side lobes) [10,17].

Investigating the impact of these dynamic effects on the encoding capacity for sensory information requires four-dimensional characterizations, i.e., emission amplitude or sensitivity gain measured over time, two direction angles, and frequency. Data of sufficient quantity and quality for such characterizations are very difficult to obtain from live bats. Therefore, the present work has been based on two types of data sets: numerical estimates derived from detailed digital models of the natural geometries of the noseleaves and pinnae [17,22] and measurements taken from biomimetic physical prototypes (either with full details or simplified) [10,21,24]. In total, four different data sets (Fig. 1) were used as a basis for an information-theoretic analysis of the dynamics in the horseshoe bat biosonar system [25].

FIG. 1. Different sample types used to obtain acoustic far-field (beam pattern) data on the emitter and receiver dynamics of greater horseshoe bat biosonar. (a) (NN) Digital noseleaf model used for computer animation of *in vivo* dynamics followed by numerical analysis. (b) (PN) Detailed physical replica of the noseleaf created through additive manufacturing (scaled 2×). (c) (BP) Portrait of a greater horseshoe bat. (d) (NP) Digital pinna model used to recreate dynamic behavior of 3D landmarks (shown as small spheres) obtained from stereo high-speed recordings. (e) (PP) Simplified deformable physical prototype modeled after the horseshoe bat pinna (scaled 2.5×).

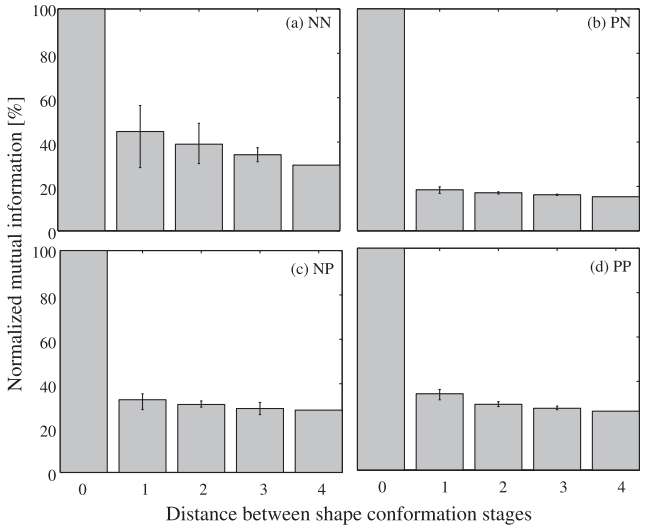

FIG. 2. Dynamic changes in noseleaf and pinna shapes result in a sequence of device characteristics (beam patterns) with low dependence as measured by mutual information. Bar height indicates normalized mutual information (in %) as a function of distance between the respective shape conformations (averaged over all conformation pairs with the respective separation value). Error bars indicate the maximum and minimum values for mutual information found across all pairs of conformation stages with the same distance. Distance is measured on an ordinal scale within a sample of representative conformations across the structures' deformation cycle. NN, PN, NP, PP refer to the samples shown in Fig. 1.

To test whether the dynamic shape changes could be functionally relevant, the sensory encoding performance of dynamic shape conformation sequences was compared to a static reference. Since each continuous dynamic shape progression was represented by a discretized sequence of five shape conformations, the static reference used an equal number of identical static conformations. This was done since averaging over multiple measurements (one for each conformation) with independent noise realizations improves the signal-to-noise ratio (SNR) and hence benefits the sensory encoding performance for static and dynamic conformation. To provide a specific functional advantage, the dynamics must encode additional sensory information with performance benefits that go beyond this generic SNR improvement associated with averaging over repeated measurements.

To test for the encoding of additional sensory information, estimates of normalized mutual information [26–29] were used to quantify the dependence between beam patterns associated with different noseleaf and pinna conformations. Mutual information between beam patterns was estimated based on beam pattern gain values that were mapped into a discrete alphabet using spectral clustering [30]. A mutual information of zero means that the two respective beam patterns offer entirely independent views of the environment and a value of 100% signifies complete dependence; i.e., the sensory information obtained with one beam pattern can be predicted completely from the information obtained with the other. The normalized mutual information estimates behaved similarly across all studied data sets: mutual information always decreased with increasing distance between the respective conformation stages (Fig. 2). For the beam patterns of neighboring conformation stages, it did not exceed 45% (maximum seen in sample NN, averaged over all combinations of neighboring conformations). With increasing distance between conformation stages, it decreased to values below 20% for the most distant stages. These values indicate a weak dependence between the beam patterns produced by different conformation stages and demonstrate that integrating sensory inputs across different stages encodes new, independent sensory information about the animal's acoustic environment.

To assess whether the additional information encoded by virtue of the sensor dynamics has a measurable impact on biosonar performance, an upper bound on resolving different directions of sound incidence was computed. The bound is based on the concept of Gaussian channel capacity [31] and gives the maximum number of directions that can be resolved without error over the entire direction domain. The number of resolvable directions is a global measure of resolution; since the method does not provide a distribution for the resolved directions, it is possible that the resolution would be much higher than average in some regions and lower in others. The bound was computed for a set of lower signal-to-noise ratios (SNR $\leq$ 20 dB). As expected, the maximum number of resolvable directions increased with the SNR for all shape types (NN, PN, NP, PP) and conformation stages (Fig. 3). Use of repeated measurements with the same device conformation stage and independent noise resulted in a resolution increase that is predicted by the SNR improvement (~7 dB) achieved by

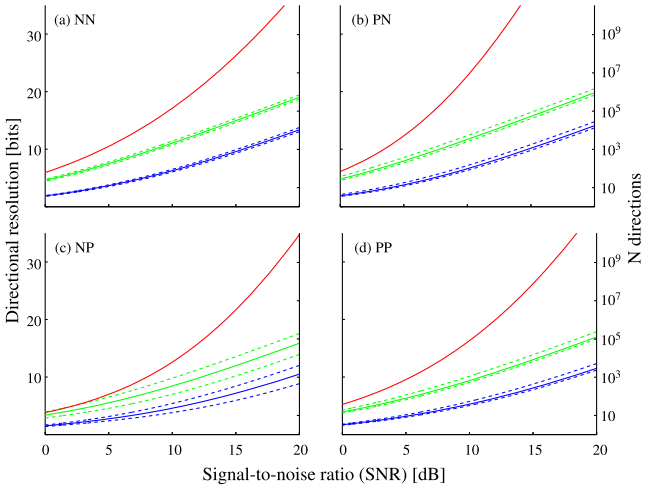

FIG. 3. Combining stages of a dynamic sensor increases the directional resolution in the presence of noise. Directional resolution is quantified by an upper bound on the number of resolvable directions that is a function of signal-to-noise ratio (additive white Gaussian noise [31]). The upper bound is expressed either directly as the maximum number of resolvable directions (right-hand axis) or as a directional resolution (in bits, i.e., $\log_2$ of the maximum number of resolvable directions, left-hand axis). Black: individual sensor conformation stages; dark gray: effect of averaging signals from an identical sensor conformation stage five times; light gray: effect of combining five different sensor conformation stages. NN, PN, NP, PP refer to the samples as shown in Fig. 1.

averaging five samples with independent noise. In contrast, combining sensory information across different conformation stages yielded resolution improvements that were substantially higher than the effects of averaging over repeated measurements from the same device conformation. As the SNR increased, the gap between the resolutions provided by averaging and those achieved by integration across different conformation stages widened. At an SNR of 6 dB, for example, a single measurement with an individual device conformation yielded a resolution of 3.7 bits (i.e., ∼13 different directions) on average. Five measurements from identical conformations improved the upper resolution bound to 7.5 bits (i.e., ∼181 resolvable directions). Combining measurements across five different conformations added another 3.5 bits of resolution and brought the total number of resolvable directions up to ∼1867. This effect was even stronger at a higher SNR of 12 dB where using different conformations improved the resolution bound by 9.5 bits over repeated measurements with identical configurations, which corresponds to increasing the upper bound on the number of resolvable directions from 3100 to 2.2×10^6.

As a complementary evaluation of how the increased sensory encoding capacity added by the shape dynamics can impact sensory estimation performance, the local accuracy of direction finding was measured by the Cramér-Rao lower bound (CLRB, [32,33]) at a higher SNR (i.e., 40 dB, Fig. 4). The CRLB provides a lower bound on the estimation error of an unbiased estimator for target direction. As a local measure, it gives a spatially resolved characterization of system performance. For each direction in space, an error ellipse can be computed which encloses the set of direction within which a certain percentage of the estimates will fall. As was the case for global bound on direction resolution described above, the CRLB performance bound was substantially improved by combining information collected across different conformation stages. In all studied data sets, the maximum value for the lower bound on the standard deviation of the estimate, i.e., the length of the major axis of the error ellipse, was reduced by between 21% (sample NN) and 38% (sample NP) on average when different conformations instead of a single repeated conformation were used (Fig. 4). In two of the four studied samples (PN and NP), use of the dynamic conformation sequence substantially reduced the right-hand (i.e., large-error) tail of the error distribution (Fig. 4). Hence, the sensor dynamics resulted in a substantial improvement of direction-finding accuracy, especially in regions where large uncertainties remained with the static configurations of the shapes.

The results of the present study demonstrate that dynamic conformation changes of the noseleaves and pinnae as seen in horseshoe bats increase the coding capacity for sensory information substantially. Since this result is based on a discretized version of the continuous shape conformation sequence seen in Nature, it is likely an underestimate of the true dynamic enhancement of the sensory encoding capacity.

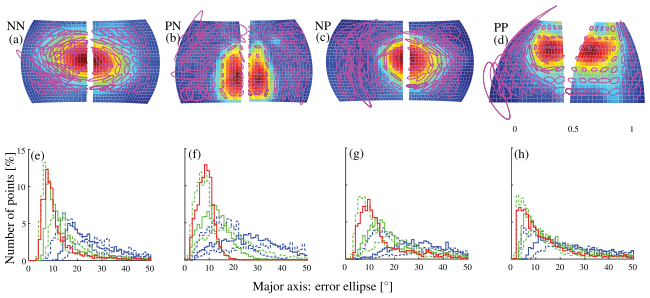

FIG. 4. Combining dynamic sensor conformations increases directional accuracy. Estimation accuracy quantified by Cramér-Rao lower bound (CRLB). Top row: map of error ellipses (90% confidence intervals) for repeated individual sensor conformation stage (left-hand side) and combination of five different sensor conformation stages (right-hand side). Error ellipses are drawn on top of the averages over all beampatterns gains used in the respective scenario. Bottom row: distribution of accuracy (major axis of the error ellipses for the 90% confidence interval). Blue: individual sensor conformation stages, green: effect of averaging the same stage five times, red: effect of using five different sensor conformation stages. NN, PN, NP, PP refer to the samples as shown in Fig. 1.

It is noteworthy that the observed effects on the sensory encoding capacity and estimation performance were qualitatively and quantitatively similar across all four data sets—despite their very different nature (i.e., physical versus numerical, detailed versus simplified). The presence of the coding-capacity effects in data obtained from numerical predictions as well as from physical measurements renders it unlikely that these results were due to methodological artifacts, since the two methods used have little in common and should hence not be subject to the same artifacts. The presence of the effects in detailed reproductions of biological shape geometries as well as in highly simplified biomimetic models suggests that the results reflect robust fundamental properties of the sensor dynamics that are not overly sensitive to the fine-scale details of the noseleaf or pinnae. This robustness of the effects will be important for potential engineering applications, because it suggests that the fundamental dynamic encoding phenomena could be exploited in manmade sensing systems even if these differed substantially from the specific biological conformations that inspired them. Nevertheless, a detailed analysis of the dynamic shape features seen in horseshoe bats could result in further improvements of the sensory-coding capacity.

Here, the utility of the dynamic effects has been demonstrated in the context of traditional sonar sensing tasks (direction resolution and direction-finding accuracy). While these tasks can be expected to be of pivotal importance to any (bio)sonar system, they are almost certainly insufficient to explain how biosonar meets the bats' sensory information needs in complicated natural environments. As of now, it remains unknown how biosonar supports the navigation of horseshoe bats in their natural environments. This leaves the intriguing possibility that the dynamics of horseshoe bat biosonar is a key factor behind some of the animals' most astounding sensory capabilities that have yet to be understood and reproduced by engineered systems. Examples of the latter are the abilities of bats to navigate in dense natural vegetation [34,35] or to fly and hunt in dense swarms. Since the dynamic effects analyzed here add an additional temporal dimension to the sensors, they could provide novel ways to address the challenges associated with these and other sensing tasks. If this is the case, bioinspired dynamic principles could allow manmade sensor technology to master the same challenges and hence close the remaining performance gap between active sensing in biology and in engineering.

This work was supported by National Aeronautics and Space Administration (Grant No. NNX09AU54G), U.S. Army Research Office (Grant No. 451069), National Science Foundation (Grants No. 1053130 and No. 1362886), Naval Engineering Education Center, National Natural Science Foundation of China (Grants No. 11374192, No. 11074149, and No. 11574183), and Fundamental Research Fund of Shandong University (Grant No. 2014QY008).

L. G. shared numerical beam pattern data, N. R. advised on clustering methods, and D. W. helped with digital animation. R. M. and A. K. G. contributed equally to this work.

*Also at Shandong University—Virginia Tech International Laboratory, Shandong University, Jinan, China.

[1] G. Neuweiler and E. Covey, *Biology of Bats* (Oxford University Press, Oxford, 2000).
[2] B. Møhl, in *Animal Sonar*, edited by P. Nachtigall and P. Moore, NATO ASI Science Vol. 156 (Springer, New York, 1988), pp. 435–450.
[3] J. Simmons, J. Acoust. Soc. Am. **54**, 157 (1973).
[4] J. A. Simmons, W. A. Lavender, B. A. Lavender, C. A. Doroshow, S. W. Kiefer, R. Livingston, and A. C. Scallet, Science **186**, 1130 (1974).
[5] J. Ostwald, H.-U. Schnitzler, and G. Schuller, in *Animal Sonar*, edited by P. Nachtigall and P. Moore, NATO ASI Science Vol. 156 (Springer, New York, 1988), pp. 413–434.
[6] M. Bates, J. Simmons, and T. Zorikov, Science **333**, 627 (2011).
[7] R. Müller, J. Acoust. Soc. Am. **128**, 1414 (2010).
[8] C. Csorba, P. Ujhelyi, and N. Thomas, *Horseshoe Bats of the World* (Alana Books, Bishop's Castle, Shropshire, England, 2003).
[9] S. Pedersen and R. Müller, *Bat Evolution, Ecology, and Conservation* (Springer Science+Business Media, New York, 2013), pp. 71–92.
[10] M. Pannala, S. Meymand, and R. Müller, Bioinspir. Biomim. **8**, 026008 (2013).
[11] R. Müller, Eur. Phys. J. Spec. Top. **224**, 3393 (2015).
[12] J. Mogdans, J. Ostwald, and H.-U. Schnitzler, J. Acoust. Soc. Am. **84**, 1676 (1988).
[13] P. Jen, Frontiers of biology **5**, 128 (2010).
[14] L. Feng, L. Gao, H. Lu, and R. Müller, PLoS One **7**, e34685 (2012).
[15] W. He, S. Pedersen, A. Gupta, J. Simmons, and R. Müller, PLoS One **10**, e0121700 (2015).
[16] H. Schneider and F. P. Möhres, J. Comp. Physiol. A **44**, 1 (1960).
[17] L. Gao, S. Balakrishnan, W. He, Z. Yan, and R. Müller, Phys. Rev. Lett. **107**, 214301 (2011).
[18] N. Matsuta, S. Hiryu, E. Fujioka, Y. Yamada, H. Riquimaroux, and Y. Watanabe, J. Exp. Biol. **216**, 1210 (2013).
[19] L. Göbbel, Cells Tissues Organs **170**, 39 (2002).
[20] A. Gupta, D. Webster, and R. Müller, J. Acoust. Soc. Am. **138**, 3188 (2015).
[21] Y. Fu, P. Caspers, and R. Müller, Bioinsp. Biomim. **11**, 036007 (2016).
[22] A. K. Gupta, Y. Fu, and R. Müller, in *ASME Conference on Smart Materials, Adaptive Structures & Intelligent Systems (SMASIS 2013)* (ASME, New York, 2013).
[23] S. Z. Meymand, M. Pannala, and R. Müller, J. Acoust. Soc. Am. **133**, 1141 (2013).
[24] R. Müller, M. Pannala, O. P. K. Reddy, and S. Z. Meymand, Smart Mater. Struct. **21**, 094025 (2012).

[25] See Supplemental Material at http://link.aps.org/supplemental/10.1103/PhysRevLett.118.158102 for description of methods and example videos of biological and biomimetic pinna and noseleaf motions.
[26] T. Cover and J. Thomas, *Elements of Information Theory* (Wiley Series in Telecommunications, Wiley, New York, 1991).
[27] C. E. Shannon, Bell Syst. Tech. J. **27**, 379 (1948).
[28] G. Basharin, Theory Probab. Appl. **4**, 333 (1959).
[29] R. Suzuki, J. Buck, and P. Tyack, J. Acoust. Soc. Am. **119**, 1849 (2006).
[30] U. V. Luxburg, Stat. Comput. **17**, 395 (2007).
[31] J. Buck, *Proceedings of the IEEE SAM Workshop* (IEEE, New York, 2002), p. 184.
[32] S. M. Kay, *Estimation Theory*, Fundamentals of Statistical Signal Processing Vol. I (Prentice Hall PTR, New Jersey, 1993).
[33] R. Müller, H. Lu, and J. R. Buck, Phys. Rev. Lett. **100**, 108701 (2008).
[34] G. Neuweiler, W. Metzner, U. Heilmann, R. Rübsamen, M. Eckrich, and H. Costa, Behav. Ecol. Sociobiol. **20**, 53 (1987).
[35] R. Müller and R. Kuc, J. Acoust. Soc. Am. **108**, 836 (2000).